Reaction Chemistry & Engineering

Accepted Manuscript

ROYAL SOCIETY OF CHEMISTRY

rsc.li/reaction-engineering

View Article Online
DOI: 10.1039/C8RE00158H

Continuous Hydrothermal Flow Synthesis of Graphene Quantum Dots

Suela Kellici,[a,*] John Acord,[b] Nicholas P. Power,[c] David J. Morgan,[d] Tobias Heil,[e] Paolo Coppo,[f] Vesna Middelkoop,[g] Ioan-Alexandru Baragau,[a] Katherine E. Moore[h] and Colin L. Raston[h]

[a] School of Engineering, Advanced Materials Research Centre, London South Bank University, 103 Borough Road, London, SE1 0AA, UK. *E-mail: kellicis@lsbu.ac.uk

[b] School of Applied Sciences, London South Bank University, 103 Borough Road, London, SE1 0AA, UK

[c] School of Life Health & Chemical Sciences, Open University, Walton Hall, Milton Keynes, MK7 6AA, UK

[d] Cardiff Catalysis Institute, School of Chemistry, Cardiff University, Park Place, Cardiff, CF10 3AT, UK

[e] Department of Colloid Chemistry, Max Planck Institute of Colloids and Interfaces, 14424 Potsdam, Germany

[f] Department of Chemistry, University of Warwick, Gibbett Hill, CV4 7AL, Coventry, UK

[g] Flemish Institute for Technological Research - VITO, Boeretang 200, B-2400 Mol, Belgium

[h] Centre for NanoScale Science and Technology, College of Science and Engineering, Flinders University Sturt Road, Bedford Park, Adelaide, SA 5042, Australia.

ABSTRACT

Green fluorescent graphene quantum dots (GQD) have been synthesized *via* hydrothermal fragmentation using a Continuous Hydrothermal Flow Synthesis (CHFS) process as a single, rapid and environmentally benign method. This is in the presence of p-phosphonic acid calix[4]arene which enhances the optical properties of the graphene quantum dots through surface functionalization, with photoluminescence quantum yields of up to 4.5%. Potential environmental impact of a lab-scale supercritical CHFS process compared with that of conventional batch processing of GQDs has been assessed using the method of the International Reference Life Cycle Data System.

View Article Online
DOI: 10.1039/C8RE00158H

INTRODUCTION

Graphene is a 2-dimensional (2D) nanomaterial with single atomic thickness and infinite lateral dimensions[1,2] which has attracted a prodigious amount of research and commercial interest from across academia and industry. However, its potential in the development of a wealth of derivatives, including graphene quantum dots, with outstanding properties such as high surface area, quantum confinement fluorescence, excellent electrical and thermal conductivity, faces limitations from not only the varying complexities involved with the technical aspects of their synthesis, but also from the associated economic and environmental costs.

Graphene, a zero-band-gap material, does not show any luminescence, but when reduced to nano-sized particles (<10 nm) it displays luminescence on excitation which can be assigned to its quantum confinement and edge effects as graphene quantum dots (GQD).[3,4] Optical properties of GQDs can be adjusted by controlling the size of the nanoparticles, surface defects, and surface functionalities.[5] Controlling the optical properties of GQDs along with imparting high stability offers scope for utilizing them in the next-generation photovoltaics, in delivering less toxic, efficient and an economically viable replacement to the currently expensive and often toxic quantum dots semiconductors. Furthermore, due to their low cytotoxicity, GQD have also found application in the biomedical field for example in bio-tagging and bio-sensing.[6,7]

Current synthetic methods for GQD use top-down (hydrothermal cutting, surface passivation, *etc.)*[5–7] and bottom-up approaches (wet chemistry or carbonization)[9,10] but they have common challenges. These include long reaction times (up to 32 hours), the use of exotic reagents, and unusual or complicated reaction conditions and processing parameters, along with issues of reproducibility. In consequence, applying these methods to an industrial scale, with high economic and environmental costs, could make them prohibitive. In this context, overcoming the

View Article Online
DOI: 10.1039/C8RE00158H

aforementioned challenges in providing new modifications in a well-controlled preparation of high-quality GQD is important. This includes bespoke tailoring for on-demand functional properties along with the reduction of surface defects that will enhance their properties and consequently their applications.

Overall, improved, rapid, tuneable, readily scalable, cleaner, and economical synthetic approaches are needed. In this vein, supercritical fluid technologies, as highlighted in the reviews by Darr and Poliakoff[11] and by Adchiri *et al.*[12] are universally accepted as offering greener, more sustainable process chemistry.[13] Their use has also been given further impetus by a more recent report on a life-cycle assessment for Continuous Hydrothermal Flow Synthesis (CHFS) production of barium strontium titanate nanoparticles[14] and titanium dioxide.[15] In this context, and in view of the "IMPROVEMENTS PRODUCTIVELY" principles of green chemistry and engineering,[16] CHFS methodology offers significant advantages over conventional synthetic routes including batch hydrothermal processes.

In this paper, we report the development of a method that enables hydrothermal fragmentation of graphene oxide sheets *via* CHFS to produce water-soluble GQD with tuneable properties. In addition, we report a life-cycle assessment for the process to highlight its green chemistry credentials (environmental benefits over traditional methodologies).

As in the synthesis of barium strontium titanate, titanium dioxide and many other materials,[13–15] it is expected that the synthesis of GQD via the CHFS system will achieve, (i) a reduction from a multistep process to a rapid single step, (ii) a significant decrease in reaction times to seconds rather than hours required for batch processes, thereby minimizing energy consumption, (iii) promote the use of safe, environmentally benign reagents and solvent (water), (iv) minimise waste (the mild basic aqueous solution can be reused through the system again or neutralised to give an

View Article Online
DOI: 10.1039/C8RE00158H

environmentally benign salt solution), and (v) provide greater control over reaction parameters (e.g. temperature and pressure) and hence particle properties. CHFS processing offers a pathway to high throughput processing,[13,17-19] allowing rapid production and evaluation of new nanocomposites. Importantly such flow processing is readily scalable[13] and can address the above challenges.

EXPERIMENTAL

GO was synthesized using a modified Hummers method from graphite.[20]

Calix[4]arene tetraphosphonic acid (PCX4) was synthesized *via* adaptation of previously reported methods[21] . The as-synthesised GO and PCX4 were then used as precursors for the synthesis of GQD in an alkaline medium via CHFS.

CHFS experiments were conducted using a flow reactor engineered as reported previously.[20] The system (simplified schematic of which is shown in Figure 2), is constructed with 316SS Swagelok stainless steel fittings and tubing. It consist of a custom-made pre-heater (labelled as "H"), three Gilson 307 HPLC pumps (labelled as "P") used for the delivery of aqueous solution of reagents, reactor (labelled as "R'), a cooler ("C") and a back-pressure regulator (BPR). The reagent delivery flow rates used were 20/5/5 mL min^{-1} for Pump 1 (delivering DI water through heater), Pump 2 (pumping pre-sonicated aqueous GO dispersion) and Pump 3 (delivering pre-mixed PCX4 and KOH solution), respectively. In a typical experiment, PCX4 (40 mg) was added to KOH (0.2 M, 40 mL) which was pumped via Pump 3 to meet a flow of a pre-sonicated (30 min) aqueous solution of GO (20 mg) dispersed in DI water (40 mL), at a T-junction ("T" in Fig. 2). This mixture then meets superheated water (450 °C, 24.8 MPa) inside a counter-current mixer (R in Fig. 2), whereupon the product formation occurred in a continuous mode. The aqueous suspension was

View Article Online
DOI: 10.1039/C8RE00158H

cooled through a vertical cooler (C) and the slurries were collected from the exit of the BPR. For the purpose of the routine synthesis of graphene materials for further use, it is possible to perform the CHFS with long operation lifetime under the same operating conditions yielding results that are consistent with the short-time scans described in this paper. The performance of the CHFS rig did not degrade during synthesis (in up to 10 hours investigated). The obtained products were filtered using a polycarbonate membrane (0.22 micron). The supernatant solutions were subjected to dialysis for 24 hrs. After dialysis, the cleaned solutions were then freeze-dried obtaining powders for further characterization.

Cellular toxicity test - The macrophage cell line RAW 264.7 (ATCC TIB-71) was grown in fully supplemented Dulbecco's modified Eagle medium (DMEM) containing 10% foetal calf serum, 100 U mL^{-1} penicillin and 100 μg mL^{-1} streptomycin. Cells were seeded in 96 well tissue-culture treated microtitre plates at a density of 5 x 10^4 cells per well and allowed to grow for 24 hrs in an incubator (37 °C, 5% CO_2) before the sample being tested was added. Samples were added to final concentrations ranging from 2 mg mL^{-1} to 31.25 μg mL^{-1}. After 24 hrs incubation with the sample, cell viability was tested using the 3-(4,5-dimethylthiazol-2-yl)-2,5-diphenyltetrazolium bromide (MTT) assay. MTT dissolved in phosphate buffered saline was added to each well at a final concentration of 1 mg mL^{-1} and the plate was returned to the incubator for 3 hrs. The media was then aspirated and 100 μL DMSO added to each well. The plate was shaken for *ca.* 10 mins at room temperature and the optical density (OD) measured at 544 nm. Cell viability was reported as a percentage value compared to untreated cells and was given by the formula: cell viability (%) = ($OD_{treated}/OD_{control}$) x 100%, where treated cells are those that were incubated with sample being tested and control cells were incubated under the same conditions but in the absence of any sample.

View Article Online
DOI: 10.1039/C8RE00158H

Each sample was performed in triplicate and the experiments were repeated twice. Results shown are the mean values and error bars represent standard deviation.

Equipment and techniques: Freeze-drying was performed using a Heto PowderDry PL 3000. A JEOL 2010 and 2100F TEM (200 kV accelerating voltage) were used for generating images of particles. XPS measurements were performed using a Kratos Axis Ultra DLD photoelectron spectrometer utilizing monochromatic Alka source operating at 144 W. Samples were mounted using conductive carbon tape. Survey and narrow scans were performed at constant pass energies of 160 and 40 eV, respectively. The base pressure of the system was ca. $1x10^{-9}$ Torr rising to *ca.* $4x10^{-9}$ Torr under the analysis of these samples. FT-IR spectra were recorded using a Nicolet Avatar 370DTGS spectrometer fitted with a Smart Orbit accessory (diamond 3000-200 cm^{-1}). A Perkin Elmer spectrometer was used for fluorescence measurements of the samples analyzed at equivalent concentrations unless otherwise stated. TGA analyses were conducted on a TGA Q500 instrument under a constant flow of nitrogen at a heating rate of 10 $°min^{-1}$ from room temperature to 800°C. UV-Vis data of dispersions of known concentrations were recorded using a UV-1800 Shimadzu UV-Vis instrument. AFM measurements were acquired using a Bruker Dimension FastScan AFM with NanoScope V controller, NanoScope control software (version 8.15) and ScanAsyst Air cantilevers (resonant frequency ≈ 70 kHz, spring constant ≈ 0.4 N/m). The peak-force tapping imaging mode was used with a scan rate of 1 Hz, set point of 500 pN, feedback gains of 1.5 and Z-limit of 0.5 µm. Data was analyzed using the NanoScope Analysis software (version 1.4). Samples were prepared for AFM by spin coating 10 µL of dilute aqueous suspension onto 1 x 1 cm freshly cleaved mica surfaces at an rpm of 1800 for 60 seconds using a 150 mm Spin Coater (Laurell Technologies Corporation).

View Article Online
DOI: 10.1039/C8RE00158H

The quantum yields of photoluminescence were measured using a solution of fluorescein in spectroscopic ethanol as a standard (Φ = 79%)[22] with an optical density of 0.08 at the excitation wavelength (420 nm). Samples A-D were suspended in distilled water up to an optical density (A) of 0.05-0.1 at 420 nm. The suspensions were analyzed in PMMA fluorescence cuvettes of 10 mm optical path. The absorption spectra were collected with a Perkin Elmer Lambda 650 C spectrophotometer and the emission spectra were collected with a Horiba Fluorolog 3 fluorimeter. The quantum yields were calculated using the equation below. The refractive indexes of the solvents were sourced from the manufacturer's specifications.

$$\phi_s = \frac{Abs_R}{Abs_s} \cdot \frac{Area_s}{Area_R} \cdot \frac{n_s}{n_R} \cdot \phi_R$$

Life-Cycle Assessment (LCA): *A life-cycle assessment* was undertaken to compare the environmental sustainability and the resource effectiveness of two processes: the production of GQD by the CHFS process and by the conventional batch processing route.[23-25] The relevant life-cycle data were investigated and compared using SimaPro (8.3.0.0) software from PRé with the Ecoinvent 3 Life Cylce Inventory database. For the calculation of the environmental impacts the ILCD 2011 Midpoint+ method was chosen (for use in PEF/OEF pilots, V1.04 / EU27 2010).

RESULTS AND DISCUSSION

We now report the synthesis of GQD in an alkaline medium using CHFS as an in situ process with p-phosphonic acid calix[4]arene[26] which controls and enhances the optical properties of GQDs, as shown in Figure 1. We have previously reported on the CHFS synthesis of GQD, as an in situ process with p-sulfonic acid-calix[4]arenes (SCX4) which is effective in controlling particle

View Article Online
DOI: 10.1039/C8RE00158H

size and optical tuning.[27] The present study provides insight into the role of the calixarene bearing sulfonic acid moieties versus phosphonic acid moieties.

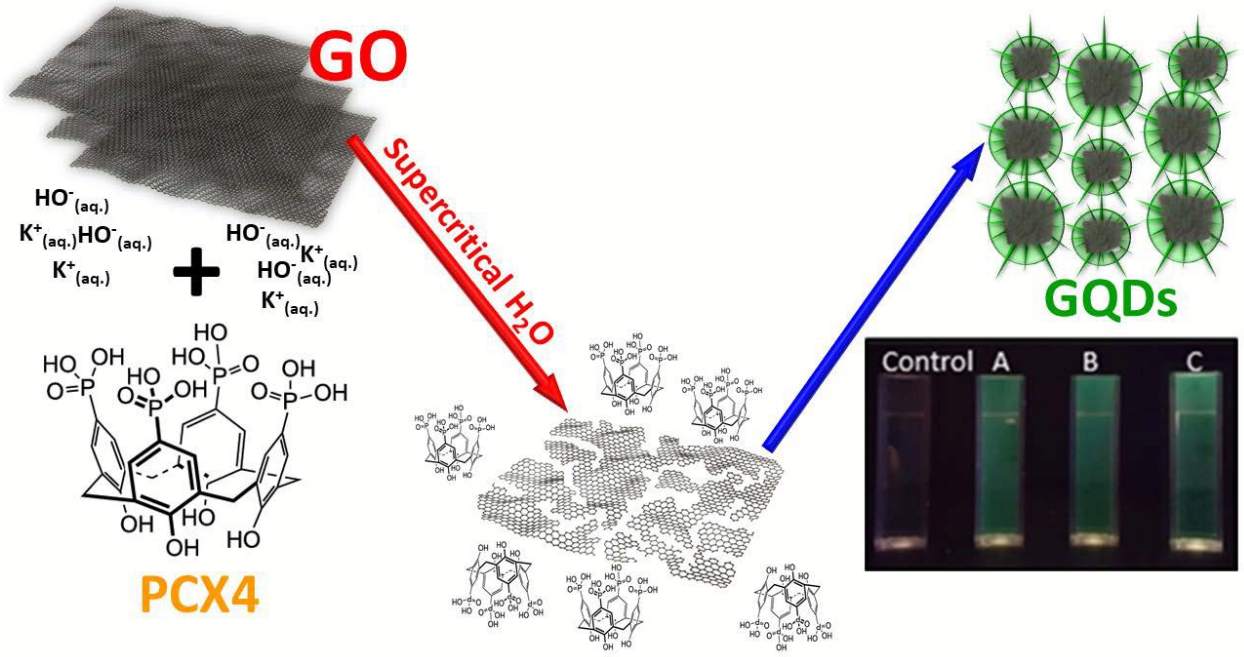

Figure 1: Schematics of the synthesis of graphene quantum dots (GQDs) from graphene oxide (GO) in the presence of p-phosphonic acid calix[4]arene (PCX4).

Calix[n]arenes typically have a cavity-shaped architecture arising from a cyclic arrangement of [n] phenol molecules linked through methylene bridges ortho- to the hydroxy group with the cavity maintained through intramolecular hydrogen bonding of the lower rim hydroxy groups. Calix[n]arene derivatives have been utilized as molecular tools for many applications, including as surfactants for both p-sulfonated[27] and p-phosphonated calix[n]arenes,[21,29,30] as well as templating and nanoparticle stabilizing agents, and the intercalation, delamination and morphological control of 2D MXenes.[31]

Continuous Hydrothermal Flow Synthesis (CHFS) provides a simple and rapid route for producing nanomaterials by mixing (in a reactor) a continuous stream of supercritical water (374

View Article Online
DOI: 10.1039/C8RE00158H

°C, 22.1 MPa) with a continuous stream of water-soluble precursor(s). CHFS represents a very fast chemical process which can assure fine control of the process parameters such as T and P, both of which can influence supersaturation and nucleation.[11–13,20] This type of process has many advantages, such as short and non-complex processes, reduced potential for requiring explosive, harmful or toxic levels of reagents or solvents, while effectively and significantly reducing the reaction time to less than one minute, and allowing continuous production of the GQD.

The process herein (see CHFS schematic in Figure 2), involves pumping a pre-sonicated aqueous dispersion of GO into a flow of a pre-mixed aqueous solution of p-phosphonic acid calix[4]arene (PCX4) and KOH (0.2 M) at room temperature through a T-junction ('T'). This mixture was then brought into contact with supercritical water (450 °C, 24.8 MPa) in a counter-current 'Reactor', whereupon the "chemical cutting" and surface functionalization of graphene oxide single-layer sheets occurred.

To investigate the influence of PCX4 on the physical and optical properties of the GQD, the concentration of PCX4 was varied from zero (Sample Control), to factors of 1, 3 and 10-fold (samples A–C respectively, Figure 1), whilst all other experimental conditions were kept constant.

View Article Online
DOI: 10.1039/C8RE00158H

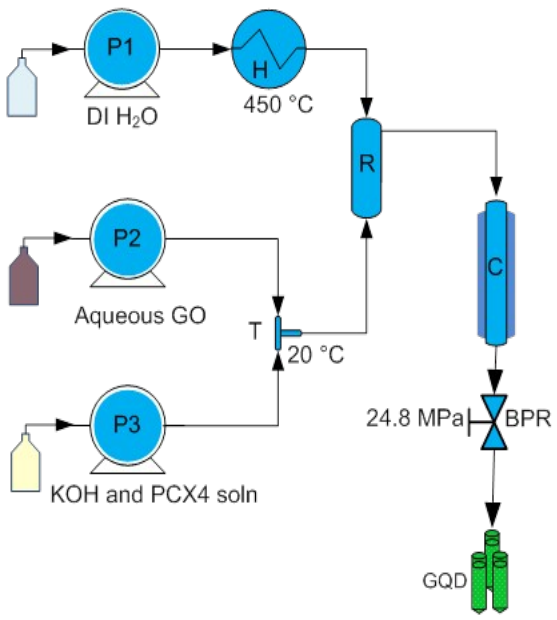

Figure 2: Schematic of the CHFS reactor employed for the synthesis of GQD. Legend: (P) HPLC delivery pump, (H) heater, (T) T-junction, (R) reactor, (C) cooler, and (BPR) back-pressure regulator

View Article Online
DOI: 10.1039/C8RE00158H

Atomic force microscopy height analysis was conducted on the GQD control sample, as well as those formed in different concentrations of PCX4, by spin coating aliquots of dilute aqueous solution onto freshly cleaved mica. AFM of the atomically flat, clean mica can be seen in Figure S1 of the Supplementary Information. Figure 3(a) depicts the height image of the GQD control sample, where the nanoparticles are individually dispersed with an average diameter of 13.8 nm. The cross sections in Figure S2 (b) shows the height profiles of two individual GQDs that are sub-nanoscale, with a sample average of 0.36 nm which is in excellent agreement with the theoretical value of 0.34 nm found in graphite.

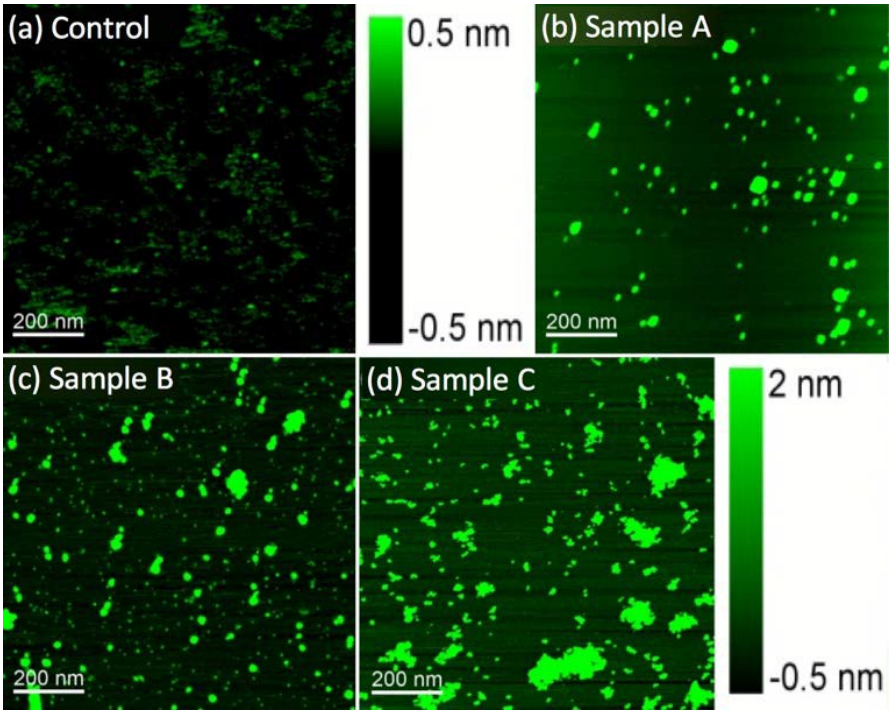

Figure 3: Images produced through the AFM analysis at a scan size of 1 x 1 µm of the control sample (scale bar -0.5-0.5 nm) and samples A–C including their respective scale bars (-0.5-2nm), showing the height of the particles.

View Article Online
DOI: 10.1039/C8RE00158H

However, such values typically range from 0.6 to 1 nm due to the presence of some residual oxygen functionalities on the sheets, such as surface hydroxyl and epoxide groups.[32] For instance, GQD synthesized through the hydrothermal cutting of oxidized graphene sheets result in heights mostly between 1 and 2 nm with only a small portion consisting of a single graphene layer, which have been defined for heights less than or equal to 1 nm.[33] Similarly, a bottom–up carbonization method with citric acid yielded heights ranging between 0.5 and 2 nm with an average of 1.4 nm.[34] The strong correlation between the GQD heights measured in this work and the literature values of graphite suggest that the GQDs are highly ordered with little to no oxygen functionality. This is consistent with XPS and TGA data as well as with our earlier reports evidencing that the treatment with KOH and supercritical water is effective in reducing the GO.[20,21,28]

Upon introduction of PCX4 (Sample A), the GQDs appear dramatically different with an increase in height up to an average of 2.89 nm, see Figure S2 (d). This increase in height with the addition of PCX4 is not unexpected as it forms 1.107 nm thick bilayers around the GQD, normal to the crystallographically observed four-fold symmetry axis running through each calixarene.[21,26,27,35] Thus, a single GQD (0.362 nm thick) is surrounded by 2 PCX4 bilayers with an additional height of 2.21 nm. Figures 3 (b) and S2 (c) show the functionalized GQD remain highly dispersed and individualized with cross-section (shown in Figure S2 (d), supplementary information) heights of 1.88 nm, 2.55 nm, and 2.72 nm. Based on theoretical heights, these may correspond to two layers of graphene and a single PCX4 bilayer, a single graphene layer between 2 PCX4 bilayers and either one or two graphene layers between two bilayers of PCX4, respectively. The functionalized GQD have an average diameter of 16.14 nm, larger than that measured for the GQD control and the transmission electron microscopy (TEM) measurement (see the Figure S3 from Supplementary Information) for Sample A, which is considerably less (2.80 ±

View Article Online
DOI: 10.1039/C8RE00158H

0.58 nm). This apparent increase in diameter may stem from dilation effects as the AFM tip traverses from the top of the nanoparticle to the base, where the higher the object, the more exaggerated the apparent dilation. This explains the significant diameter difference upon addition of PCX4, which is unlikely to assemble upon the edge planes of the GQD, but results in a dramatic increase in height. Alternatively, the dilation may also be an artifact of the particle analysis process (see Figure S4 of the Supporting information for a brief explanation of particle analysis). This discrepancy in diameter between AFM and TEM is apparent and consistent with all samples analyzed.

When the concentration of PCX4 was increased by a factor of three, as in Sample B, AFM height images showed a very different topography. Figures 3(c) and S2(e) show a mixture of larger (≈ 4 – 5 nm) and smaller (≈ 1.5 – 2 nm) individualized particles, with an average height of 2.21 nm (and diameter of 15.72 nm). Previous studies on PCX4 have identified the formation of nanorafts as small as 3 nm, which assembly underflow in a spinning disk processor.[26] This suggests that the very small particles observed in the present work correspond to PCX4 nanorafts devoid of GQD, theoretically having a height of 2.21 nm. The larger particles may consist of multiple graphene layers interlaced with bilayers of PCX4 or surrounded by only 2 bilayers. For instance, two and three GQD layers interlaced with PCX4 would correspond to theoretical heights of 4.04 nm and 5.63 nm, respectively, and two and three GQD layers surrounded only by two PCX4 bilayers would correspond to heights of 2.89 nm and 3.23 nm, respectively.

Lastly, the 10-fold concentration of PCX4 resulted in GQD particles with an average height of 3.60 nm (Figures 3 (d) and S2 (g)) and an average diameter of 17.80 nm. Cross sections are shown in Figure S2 (g) correspond to heights of 2.50 nm, 2.58 nm and 3.22 nm, which can be considered two single intercalated graphene layers and possibly a 3-layer assembly with PCX4

View Article Online
DOI: 10.1039/C8RE00158H

forming bilayers only around the outside (theoretical height 3.23 nm). All these results are supported using TEM (see SI, Figure S3). Whilst PCX4 limits particle size and narrows particle size distribution similar in effect to that imparted by SCX4, it differs however, to SCX4 in that increasing concentrations of PCX4 in the reaction did not coincide with further reduction in particle sizes.

Photoluminescence (PL) studies (see S.I. Figure S6) of aqueous solutions of each of the GQD samples were performed after it was observed that excitation at 365 nm led to a bright green fluorescence (Figure 1 inset A-C). With the excitation wavelength varied from 360-440 nm, the maximum excitation wavelength for the control sample was observed at 360 nm with the greatest emission intensity at a maximum of 420 nm, however, for samples A, B, and C, a single-emission maximum at 510 nm was observed for all excitation wavelengths between 380-440 nm (Figure 4), clearly indicating an excitation independent profile for the decorated GQD particles. Whilst the intrinsic luminescence can be attributed to the sp^2-carbon framework as well as parameters such as particle size and particle size distribution for the GQDs (Samples A-C), the control is only similar in respect to particle size and size distribution as indicated by TEM measurements (see SI). It is in the extent and variation of surface defects[5–10] (influenced by PCX4 in combination with hydrothermal cutting) along with surface decoration with the coating of layers of PCX4 that the GQDs differs to the control. The level of surface modification experienced by the GQDs, re-establishing more of their sp^2-carbon framework, was far more extensive than that for the control. This was supported by X-ray photoelectron spectroscopy (XPS) (discussed later) which also lends support to the AFM analysis that the graphene surface was decorated with PCX4, and this was in the form of bilayers. The calixarenes have enhanced the GQDs dispersion, thus preventing formation of layered aggregates in solution and thereby possibly further contributing to better

View Article Online
DOI: 10.1039/C8RE00158H

spectral emissions with excitation independent behavior as observed for Samples A-C. The quantum yield measurements for stable aqueous suspensions of GQD gave values of 4.2% (sample A), 4.5% (sample B), and 2.9% (sample C), with negligible quantum yield for the control sample. This excitation independent behavior was comparable to the in-situ generation of GQD with SCX4,[27] but unlike other GQD materials reported.

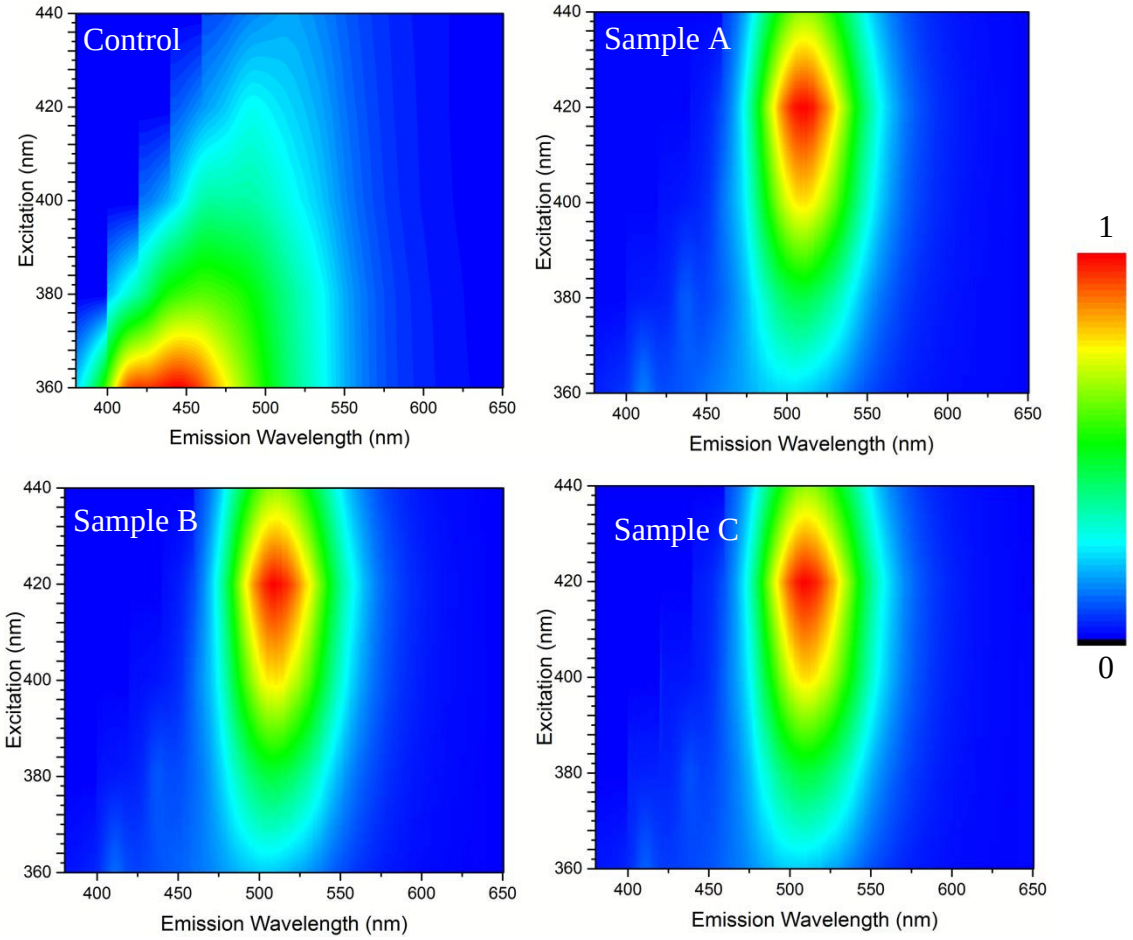

Figure 4: 2D excitation-emission contour map of GQD compounds. Normalized intensity scale bar is included.

View Article Online
DOI: 10.1039/C8RE00158H

X-ray photoelectron spectroscopy (XPS) analysis was undertaken to determine changes in the chemical states of all synthesized GQDs and PCX4, (see S.I. Figure S7). As we previously reported,[20,27,28] the precursor graphene oxide which is treated hydrothermally exhibited significantly reduced peak intensities of the oxygen-containing functional groups (epoxide, carboxyl and hydroxy). This reduction in peak intensities was further enhanced in the presence of PCX4 during the hydrothermal process. GQD samples A, B, and C have shown significant reduction for O-C peak at the O(1s) spectrum (~ 531.3 eV) compared to the control. XPS analysis for standalone p-phosphonic acid calix[n]arenes, revealed a strong P(2p) (see Figure S7) signal at 134.0 eV (± 0.2 eV), which is characteristic of the phosphorous-based calixarene.[31] The presence of PCX4 in GQD samples is reflected in the C(1s) (see Figure S7) spectrum with strong peaks for the C-C (~ 285.0 eV) and C-P (~ 286.0 eV), and the weak π-π* transitions (~ 289.0 eV) assigned to the aromatic structure present in the calixarene macrocycle. Interestingly, a negative shift from ~ 134 eV for P(2p) in PCX4 to ~ 133 eV in the GQD is observed suggesting a change in electron density for P. This can be attributed to the disruption of hydrogen bonding of the phosphonic acid units of PCX4 due to new binding interactions with graphene and/or potassium ions (from the reaction process). Such changes in energy have previously been reported for phosphoric acid activated membranes on perturbation of hydrogen bonding.[37]

PCX4 functionalized onto GO involves (a) non-covalent π- π interactions and (b) hydrogen bonding interactions between hydroxyl groups of PCX4 and oxygen functional groups of GO.[27,38] This differs to that proposed for SCX4 where the location of calixarenes on the GQD was primarily expected to be edge aligned (Lerf-Klinowski model for graphene) with SCX4's phenol moiety as part of an ester linkage formed with the GQD edge carboxylic groups, facilitated under CHFS conditions. Whilst both SCX4 and PCX4 are known to form bilayers from aqueous solution with

View Article Online
DOI: 10.1039/C8RE00158H

metal ions or other organic molecules, it is difficult to speculate as to why they differ in their interactions with graphene oxide in the synthesis of the respective GQDs.

Elemental analysis results (from XPS analysis) indicate that the GQDs are mainly composed of carbon, oxygen, phosphorous and potassium. An increase in phosphorous content was observed from 1.34% (sample "A"), 1.27% (sample "B") and highest elemental composition of 3.9% for sample “C” which has the highest nominal PCX4 concentration. This strongly suggests that PCX4 has been successfully attached to the graphene primarily through supramolecular interactions and this is further supported by FT-IR and TGA data.

FTIR spectroscopy of the samples A-C (Figure S8, supplementary information) revealed a broadening of the O-H band and a shift to ~ 3130 cm^{-1} from 3390 cm^{-1} for the control. This reflects the increased presence of hydroxyl groups introduced from the phenolic (3140 cm^{-1}) and phosphonic acid (PO-H, 2725 cm^{-1}) functionalities of PCX4 in the layers and bilayers of the GQD.[29] Bands located for the "control" sample at 1400 cm^{-1} (>COO- symmetric stretch) and 1523 cm^{-1} (>COO- asymmetric stretch) undergo a successive and significant reduction in the peak intensity with increasing PCX4 concentration in GQD synthesis for samples A-C. The reduction of the carboxylic peaks are in agreement with that observed for the XPS analysis.

Thermogravimetric analysis (TGA) evaluation revealed both the thermal stability of the PCX4 functionalized GQDs and the load bearing of GQD for PCX4 when compared to the control sample. The significant increasing weight loss, (Figure S9, supplementary information), observed in the region 400-800 °C for samples A, B, and C can be attributed to PCX4 decomposition (9.8%, 12.4%, & 13.9% respectively). Hydrogen bonding, Van der Waals interactions and π-π stacking between PCX4 and GQD is largely expected, and given the forcing conditions under CHFS processing, some covalent bonding between PCX4 and the rGO is also likely, for example as ester

View Article Online
DOI: 10.1039/C8RE00158H

linkages of the phenol moieties with the GQD edge carboxylic groups. This is consistent with XPS data observed for the C3/C4 ratio and previously reported for p-sulfonated calixarenes with rGO.[27]

UV-Vis spectroscopy (see Figure S10) of pure PCX4 shows π-π* transitions centered at *ca.* 276 and 283 nm. The new composite materials A-C have a band at *ca.* 282 nm, indicative of the presence of PCX4 in GQD. As anticipated, there was no corresponding peak for PCX4 observed for the control sample, with an absorption band at ca. 270 nm, which is consistent with literature values.[27]

Cell cytotoxicity experiments: For the evaluation of the toxicity of the hydrothermally prepared compounds against eukaryotic cells, the macrophage cell line RAW 264.7 was incubated with various concentrations of GQDs, PCX4 and control for 24 hrs. An MTT assay was performed used to determine cell viability with the results reported as % viability (MTT value of cells with compound/MTT value of cells without compound x 100) (Figure 5).

Neither the rGO control nor the PCX4, for the concentrations tested, had any significant impact on cell viability. For samples A-C, toxicity to RAW 264.7 cells is greater, in a dose-dependent manner, compared to PCX4 alone at all concentrations tested, and the percentage of cells killed by each compound is approximately similar at each concentration. It is interesting to note that in complexing rGO with PCX4 results in increased cytotoxicity. This may be explained by the rGO sheet being decorated with PCX4 molecules, resulting in an increased localized concentration of PCX4 compared to standalone PCX4. This is further reflected by samples A-C showing quite similar levels of toxicity at each concentration, regardless of the initial ratio of PCX4 to rGO used in their synthesis. Given the structural organization of the nanoparticle assemblies in samples A-C, each consisting of a graphene sheet(s) coated in a bilayer(s) of PCX4, and that each of the samples have significant overlap in their size distribution (as suggested by AFM and TEM

View Article Online
DOI: 10.1039/C8RE00158H

analysis), then the cells can be considered essentially to being just exposed to high localized concentrations of PCX4.

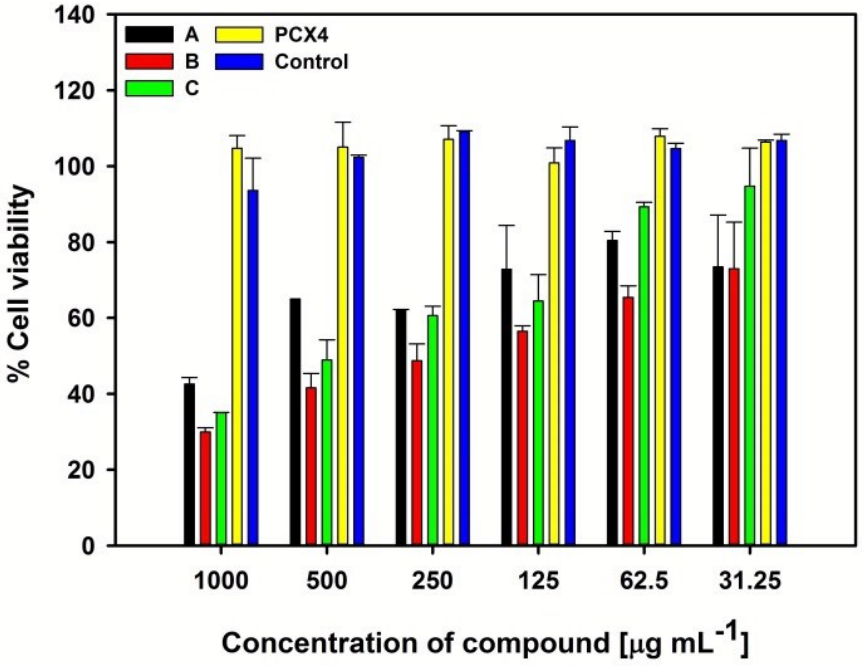

Figure 5: RAW 264.7 cell viability studies after incubation with GQD and PCX4 at varying concentrations for 24 hours.

The toxicity observed is best explained in this regard, and the observed complexities in the assemblies of the individual samples A-C have no further or significant impact. Nevertheless, at the concentrations that the composite materials will be typically used, the levels of cytotoxicity are at acceptable levels, and as such, this will not impact on the usefulness of the compounds. Earlier studies established that PCX4 has low toxicity towards PC12 cells and higher susceptibility towards toxic effects for mixed retinal cells, with cell viability reduced by 50% respectively for >3.0 and 1.0 mg mL^{-1} after 24 hours.[39]

View Article Online
DOI: 10.1039/C8RE00158H

A life-cycle assessment (LCA): The environmental impact has been evaluated across 16 separate impact categories (Figure 6) using the ILCD method. The summarized inventories are presented electronic supplementary information (Table S1). The production of starting graphene oxide powder (chemical oxidation via Hummer's method) used in the CHFS was assigned to be the same as that of the lab scale process for batch hydrothermal synthesis.

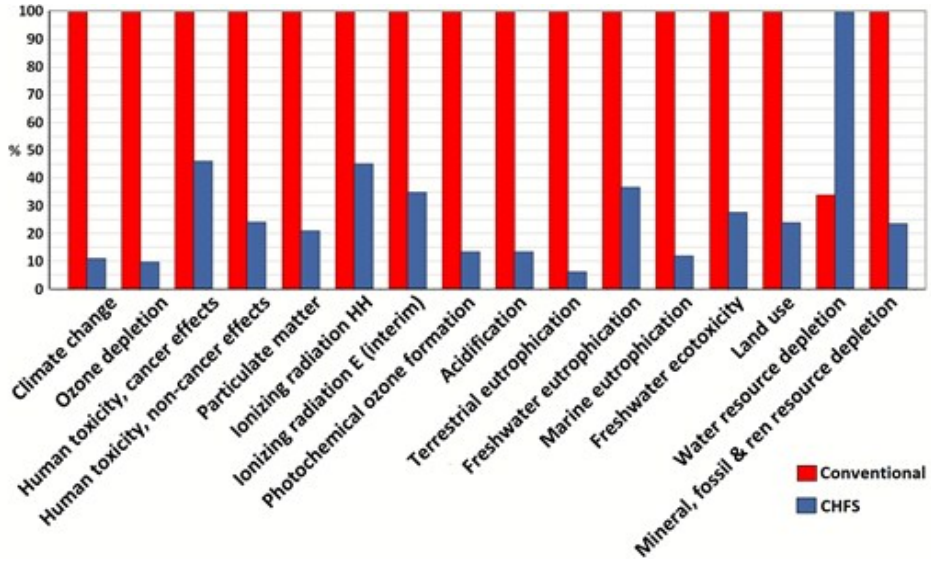

Figure 6: Comparison of the life-cycle assessment for the 1 mg GQD prepared by the conventional hydrothermal batch synthesis (red) and by CHFS (blue) showing the values pertinent to each of the 16 midpoint environmental impact categories. All values are shown in percentages while each impact category is expressed in its reference units. Legend key: red color bar - conventional method, blue bar – CHFS.

In a recent report, a comparative LCA study of different graphene production routes (graphite chemical oxidation, chemical vapor deposition and electrochemical exfoliation) indicated the chemical oxidation process (which was utilized here) has the least impacting synthetic approach to obtain large quantities of graphene.[25] It was therefore only necessary to construct the inventories

View Article Online
DOI: 10.1039/C8RE00158H

for the mass of the precursors required for the solutions. These quantities were then factored down accordingly.

The impact of the energy demand (use of electricity) of the laboratory equipment for both production processes were estimated separately. The amount of energy consumed by each piece of electrical equipment was not measured using an in-line power meter, but only calculated theoretically. It is noted (Figure S11, supplementary information) that the electricity consumption for the conventional batch synthesis is significantly higher due to the sheer duration of the reaction (24 hours as compared to 20 min of the CHFS, including the reactor reaching the required reaction temperature). Still, the disproportionately the contribution by the direct electricity consumption even during the CHFS of a single amount of the GQD material can be explained by the non-optimised lab-scale setup used in this study for synthesizing small quantities of the material. The adequately scaled-up CHFS process would employ multiple syntheses operated in parallel while using equal quantities of electricity as well as the use of heat-exchangers. The two synthetic routes do not differ from each other in the remaining steps of the preparation process (sonication, filtration) except for their precursors.

One of the key conclusions of the LCA analysis of the CHFS of GQD as previously reported for other syntheses[13–15] is that the CHFS offers a substantial degree of reduction in the overall life-cycle environmental impact (Figure S12, supplementary information). The CHFS of GQDs has a substantially lower environmental impact than the equivalent conventional batch synthesis. The values for ‘Human toxicity’, ‘Ionising radiation’ and ‘Particulate matter’, while still significant, are more moderate (at < 50 %) for the CHFS. The large contribution from the water for the CHFS is due to the water being cycled through the system for the purpose of cooling it down; however,

View Article Online
DOI: 10.1039/C8RE00158H

this water can be subsequently reused in the following runs and its environmental impact can, therefore, be effectively omitted.

CONCLUSIONS

In conclusion, a rapid continuous hydrothermal flow route was employed for the synthesis of graphene quantum dots in the presence of p-phosphonic calix[4]arene. The versatility of this synthetic route should allow the rapid synthesis of quantum dots based on the ever-expanding range of two-dimensional materials. The photoluminescence studies for the GQDs showed an excitation independent behavior with the emission peak at 510 nm. The cytotoxicity of the composite material is acceptable, and LCA studies establish that the CHSF method offers a simplified synthetic process that improves efficiency and reduces the environmental impact of the material production. Furthermore, the LCA emphasizes the potential for scale-up for the continuous production of large quantities of GQD.

CONFLICTS OF INTEREST

The authors have no conflicts of interest to declare.

ACKNOWLEDGEMENTS

SK and NP would like to thank the EPSRC Grand Challenge Network, the Directed Assembly Network, for the pump-priming award PP105 31-05-2016. SK, NP, and JA also gratefully acknowledge the financial support provided by LSBU. CLR and KEM acknowledge the facilities,

View Article Online
DOI: 10.1039/C8RE00158H

and the scientific and technical assistance, of the Australian Microscopy & Microanalysis Research Facility at Flinders Microscopy, Flinders University, and support from the Australian Research Council. The authors would like to thank Boonen Katrien for assistance with the databases within the SimaPro software.

REFERENCES

(1) Novoselov, K. S.; Geim, A. K.; Morozov, S. V; Jiang, D.; Zhang, Y.; Dubonos, S. V; Grigorieva, I. V; Firsov, A. A.; Novoselov, K. S. Electric Field Effect in Atomically Thin Carbon Films. *Source Sci. New Ser. Gene Expr. Genes Action* **2007**, *306* (5696), 183–191.

(2) Geim, A. K.; Novoselov, K. S. The rise of graphene. *Nat. Mater.* **2007**, *6* (3), 183–191.

(3) Geim, A. K. Graphene: Status and prospects. *Science*. 2009, pp 1530–1534.

(4) Dreyer, D. R.; Park, S.; Bielawski, C. W.; Ruoff, R. S. The chemistry of graphene oxide. *Chem. Soc. Rev.* **2010**, *39* (1), 228–240.

(5) Liu M L.; Yang L.;, Li R.; Chen, B B.; Liu, H.; Huang, C. Large-scale simultaneous synthesis of highly photoluminescent green amorphous carbon nanodots and yellow crystalline graphene quantum dots at room temperature. Green Chemistry, **2017**, 19(15): 3611-3617.

(6) Zhu, S.; Zhang, J.; Tang, S.; Qiao, C.; Wang, L.; Wang, H.; Liu, X.; Li, B.; Li, Y.; Yu, W. Surface chemistry routes to modulate the photoluminescence of graphene quantum dots: From fluorescence mechanism to up-conversion bioimaging applications. *Adv. Funct. Mater.* **2012**, *22* (22), 4732–4740.

(7) Li, L.; Wu, G.; Yang, G.; Peng, J.; Zhao, J.; Zhu, J.-J. Focusing on luminescent graphene

View Article Online
DOI: 10.1039/C8RE00158H

quantum dots: current status and future perspectives. *Nanoscale* **2013**, *5* (10), 4015–4039.

(8) Baker, S. N.; Baker, G. A. Luminescent Carbon Nanodots: Emergent Nanolights. *Angew. Chemie Int. Ed.* **2010**, *49* (38), 6726–6744.

(9) Shen, J.; Zhu, Y.; Yang, X.; Li, C. Graphene quantum dots: emergent nanolights for bioimaging, sensors, catalysis and photovoltaic devices. *Chem. Commun.* **2012**, *48* (31), 3686.

(10) (a) Bacon, M.; Bradley, S. J.; Nann, T. Graphene Quantum Dots. *Part. Part. Syst. Charact.* **2014**, *31* (4), 415–428. (b) Anh, N. T. N.; Chowdhury, A. D.; Doong, R. Highly sensitive and selective detection of mercury ions using N, S-codoped graphene quantum dots and its paper strip based sensing application in wastewater. Sensors and Actuators B: Chemical, **2017**, 252, 1169-1178.

(11) Darr, J. A.; Poliakoff, M. New Directions in Inorganic and Metal-Organic Coordination Chemistry in Supercritical Fluids. *Chem. Rev.* **1999**, *99* (2), 495–542.

(12) Adschiri, T.; Lee, Y.-W.; Goto, M.; Takami, S. Green materials synthesis with supercritical water. *Green Chem.* **2011**, *13* (6), 1380.

(13) Darr, J. A.; Zhang, J.; Makwana, N. M.; Weng, X. Continuous Hydrothermal Synthesis of Inorganic Nanoparticles: Applications and Future Directions. *Chem. Rev.* **2017**, *117* (17), 11125–11238.

(14) Tsang, M.; Philippot, G.; Aymonier, C.; Sonnemann, G. Anticipatory life-cycle assessment of supercritical fluid synthesis of barium strontium titanate nanoparticles. *Green Chem.* **2016**, *18* (18), 4924–4933.

(15) Caramazana-Gonzalez, P.; Dunne, P. W.; Gimeno-Fabra, M.; Zilka, M.; Ticha, M.;

View Article Online
DOI: 10.1039/C8RE00158H

Stieberova, B.; Freiberg, F.; McKechnie, J.; Lester, E. H. Assessing the life cycle environmental impacts of titania nanoparticle production by continuous flow solvo/hydrothermal syntheses. *Green Chem.* **2017**, *19* (6), 1536–1547.

(16) Tang, S. Y.; Bourne, R. A.; Smith, R. L.; Poliakoff, M. The 24 Principles of Green Engineering and Green Chemistry: "IMPROVEMENTS PRODUCTIVELY." *Green Chem.* **2008**, *10* (3), 268.

(17) Goodall, J. B. M.; Kellici, S.; Illsley, D.; Lines, R.; Knowles, J. C.; Darr, J. a. Optical and photocatalytic behaviours of nanoparticles in the Ti-Zn-O binary system. *RSC Adv.* **2014**, *4*, 31799–31809.

(18) Weng, X.; Cockcroft, J. K.; Hyett, G.; Vickers, M.; Boldrin, P.; Tang, C. C.; Thompson, S. P.; Parker, J. E.; Knowles, J. C.; Rehman, I.; et al. High-throughput continuous hydrothermal synthesis of an entire nanoceramic phase diagram. *J. Comb. Chem.* **2009**, *11* (5), 829–834.

(19) Kellici, S.; Gong, K.; Lin, T.; Brown, S.; Clark, R. J. H.; Vickers, M.; Cockcroft, J. K.; Middelkoop, V.; Barnes, P.; Perkins, J. M.; et al. High-throughput continuous hydrothermal flow synthesis of Zn-Ce oxides: unprecedented solubility of Zn in the nanoparticle fluorite lattice. *Philos. Trans. R. Soc. A Math. Phys. Eng. Sci.* **2010**, *368* (1927), 4331–4349.

(20) Kellici, S.; Acord, J.; Ball, J.; Reehal, H. S.; Morgan, D.; Saha, B. A single rapid route for the synthesis of reduced graphene oxide with antibacterial activities. *RSC Adv.* **2014**, *4* (29), 14858.

(21) Clark, T. E.; Makha, M.; Sobolev, A. N.; Su, D.; Rohrs, H.; Gross, M. L.; Atwood, J. L.; Raston, C. L. Self-organised nano-arrays of p-phosphonic acid functionalised higher order

View Article Online
DOI: 10.1039/C8RE00158H

calixarenes. *New J. Chem.* **2008**, *32* (9), 1478–1483.

(22) Kellogg, R. E.; Bennett, R. G. Radiationless intermolecular energy transfer. III. Determination of phosphorescence efficiencies. *J. Chem. Phys.* **1964**, *41* (10), 3042–3045.

(23) Arvidsson, R.; Kushnir, D.; Sandan, B. A.; Molander, S. Prospective life cycle assessment of graphene production by ultrasonication and chemical reduction. Environ. Sci. Technol. 2014, 48 (8), 4529–4536.

(24) Caramazana-González, P.; Dunne, P. W.; Gimeno-Fabra, M.; Zilka, M.; Ticha, M.; Stieberova, B.; Freiberg, F.; McKechnie, J.; Lester, E. H. Assessing the life cycle environmental impacts of titania nanoparticle production by continuous flow solvo/hydrothermal syntheses. Green Chem. 2017, 19 (6), 1536–1547.

(25) Cossutta, M.; McKechnie, J.; Pickeing J. S. A comparative LCA of different graphene production routes. Green Chem. 2017, 19, 5874-5884.

(26) Clark, T. E.; Makha, M.; Sobolev, A. N.; Rohrs, H.; Atwood, J. L.; Raston, C. L. Engineering Nanorafts of Calixarene Polyphosphonates. *Chem. – A Eur. J.* **2008**, *14* (13), 3931–3938.

(27) Kellici, S.; Acord, J.; Power, N. P.; Morgan, D. J.; Coppo, P.; Heil, T.; Saha, B. Rapid synthesis of graphene quantum dots using a continuous hydrothermal flow synthesis approach. *RSC Adv.* **2017**, *7* (24), 14716–14720.

(28) Kellici, S.; Acord, J.; Vaughn, A.; Power, N. P.; Morgan, D. J.; Heil, T.; Facq, S. P.; Lampronti, G. I. Calixarene Assisted Rapid Synthesis of Silver-Graphene Nanocomposites with Enhanced Antibacterial Activity. *ACS Appl. Mater. Interfaces* **2016**, *8* (29), 19038–19046.

View Article Online
DOI: 10.1039/C8RE00158H

(29) Martin, A. D.; Raston, C. L. Multifunctional p-phosphonated calixarenes. *Chem. Commun.* **2011**, *47* (35), 9764–9772.

(30) Hartlieb, K. J.; Saunders, M.; Raston, C. L. Templating silver nanoparticle growth using phosphonated calixarenes. *Chem. Commun.* **2009**, No. 21, 3074–3076.

(31) Vaughn, A.; Ball, J.; Heil, T.; Morgan, D. J.; Lampronti, G. I.; Maršalkaitė, G.; Raston, C. L.; Power, N. P.; Kellici, S. Selective Calixarene-Directed Synthesis of MXene Plates, Crumpled Sheets, Spheres, and Scrolls. *Chem. - A Eur. J.* **2017**, *23* (34), 8128–8133.

(32) Schniepp, H. C.; Li, J. L.; McAllister, M. J.; Sai, H.; Herrera-Alonson, M.; Adamson, D. H.; Prud'homme, R. K.; Car, R.; Seville, D. A.; Aksay, I. A. Functionalized single graphene sheets derived from splitting graphite oxide. *J. Phys. Chem. B* **2006**, *110* (17), 8535–8539.

(33) Pan, D.; Zhang, J.; Li, Z.; Wu, M. Hydrothermal Route for Cutting Graphene Sheets into Blue-Luminescent Graphene Quantum Dots. *Adv. Mater.* **2010**, *22* (6), 734–738.

(34) Dong, Y.; Shao, J.; Chen, C.; Li, H.; Wang, R.; Chi, Y.; Lin, X.; Chen, G. Blue luminescent graphene quantum dots and graphene oxide prepared by tuning the carbonization degree of citric acid. *Carbon N. Y.* **2012**, *50* (12), 4738–4743.

(35) Martin, A. Supramolecular Chemistry of Phosphonic Acid Calixarenes. **2011**.

(36) Wang, C.; Duan, Y.; Zacharia, N. S.; Vogt, B. D. A family of mechanically adaptive supramolecular graphene oxide/poly(ethylenimine) hydrogels from aqueous assembly. *Soft Matter* **2017**, *13* (6), 1161–1170.

(37) Ariza, M. J.; Rodríguez-Castellón, E.; Rico, R.; Benavente, J.; Muñoz, M.; Oleinikova, M. X-Ray Photoelectron Spectroscopy Analysis of Di-(2-ethylhexyl) Phosphoric Acid Activated Membranes. *J. Colloid Interface Sci.* **2000**, *226* (1), 151–158.

View Article Online
DOI: 10.1039/C8RE00158H

(38) Shen, J.; Zhu, Y.; Yang, X.; Zong, J.; Zhang, J.; Li, C. One-pot hydrothermal synthesis of graphene quantum dots surface-passivated by polyethylene glycol and their photoelectric conversion under near-infrared light. *New J. Chem.* **2012**, *36* (1), 97–101.

(39) Coleman, A.W.; Bott, S.G.; Morley, S.D.; Means, C.M.; Robinson, K.D.; Zhang, H.; Atwood J.L. Novel Layer Structure of Sodium Calix[4]arenesulfonate Complexes—a Class of Organic Clay Mimics? *Angew. Chem. Int. Ed. Engl*. **1988**, *27* (10), 1361-1362. Ling, I,; Sobolev, A. N.; Raston, C. L. Controlling the organization of phosphonium cations relative to p-sulfonatocalix[4]arene anions. *CrystEngComm*, **2015**, *17*, 1526-1530.

(40) Martin, A. D.; Houlihan, E.; Morellini, N.; Eggers, P. K.; James, E.; Stubbs, K. A.; Harvey, A. R.; Fitzgerald, M.; Raston, C. L.; Dunlop, S. A. Synthesis and Toxicology of p-Phosphonic Acid Calixarenes and O-Alkylated Analogues as Potential Calixarene-Based Phospholipids. *Chempluschem* **2012**, *77* (4), 308–313.

View Article Online
DOI: 10.1039/C8RE00158H

A rapid, continuous hydrothermal flow route and life cycle assessment was employed for the synthesis of graphene quantum dots in the presence of calixarene.